Tribology International 218 (2026) 111721

Contents lists available at ScienceDirect

Tribology International

journal homepage: www.elsevier.com/locate/triboint

Full Length Article

Influence of morphology on friction anisotropy of GLAD Mo films

Guilherme B. Rodrigues [a,*], Pascal Boulet [b], Nicolas Martin [a], Fabien Amiot [a], Guillaume Colas [a,*]

[a] Université Marie et Louis Pasteur, SUPMICROTECH-ENSMM, CNRS, Institut FEMTO-ST, F-25000, Besançon, France
[b] Université de Lorraine, CNRS, Institut Jean Lamour, F-54000, Nancy, France

ARTICLE INFO

Keywords:
Friction anisotropy
GLAD films
Molybdenum

ABSTRACT

Frictional behavior of molybdenum thin films deposited by Glancing Angle Deposition (GLAD) was investigated at various deposition angles (α) using single-scratch tests under different loads and directions. Films deposited at $\alpha \geq 50°$ developed elliptical columnar structures, resulting in orthotropic anisotropy due to direction-dependent plastic deformation. Increasing the deposition angle enhanced intercolumnar porosity, thereby reducing both friction and anisotropy. Conversely, the film deposited at $\alpha = 40°$ exhibited strong anisotropy and a non-Coulombic frictional response. Moreover, this film showed non-centrosymmetric behavior, requiring a non-linear model to accurately describe its frictional anisotropy.

1. Introduction

Since the first studies of friction, tribology has increasingly evolved to address complex phenomena such as friction anisotropy. This behavior, characterized by the presence of different friction responses depending on the sliding direction, can be naturally observed in single crystals [1,2], as well as in biological surfaces [3–5]. These surfaces were used as a basis for the development of various bio-inspired surfaces, which attempt to replicate them by introducing micro- and nanostructures in the surface material [6,7].

In recent decades, GLancing Angle Deposition (GLAD) has been shown to enable the creation of tilted columnar structures in thin films [8]. This technique is a Physical Vapor Deposition (PVD) version in which an additional glancing angle between the substrate and the target is applied. As a result, other phenomena, such as the so-called shadowing and fanning effects, are present and considerably influence the morphology and crystallographic aspects of the GLAD films [9]. Furthermore, by tuning deposition parameters, the nanostructures formed during the GLAD growth may be defined in a way to produce surface aspects similar to those observed on biological surfaces. However, despite this potential of the GLAD technique in obtaining friction anisotropy, studies on the mechanical and frictional properties of this type of films remain relatively limited.

In a recently published work, we have reported these limitations of the state-of-art and also showed the friction anisotropy of tungsten GLAD films by applying scratch tests in different scratching directions [10]. The anisotropic behavior is strongly dependent on morphology of the films, and consequently on the deposition angle (α). Two anisotropic behaviors were identified. The first is non-centrosymmetric (between the directions along and against the columns tilt), and the second is orthotropic (between the directions perpendicular to the atom flux and the other directions). Post-scratching investigations showed that the orthotropic response of the films deposited at $\alpha \geq 60°$ is controlled by the plastic deformation of the columns. A limited permanent deformation is observed when scratching at the direction perpendicular to the atom flux, resulting in larger friction coefficients. An analytical approach based-on a 1D mechanical model proposed in the study supports this conclusion.

In this context, the present study aims at assessing whether the occurrence and characteristics of friction anisotropy are material-dependent by applying a similar methodological approach to a different metal: Molybdenum (Mo). It is well established that molybdenum enables the formation of well-defined nanostructures at high deposition angles [11–13]. Additionally, it exhibits significant thermal and mechanical stability during thin film growth, making it suitable for various electronic and optical applications [14–17].

Thus, a series of Mo films were deposited, varying the deposition angle (α) from 0° to 85°, followed by a detailed analysis of their morphological and crystallographic characteristics. Scratch tests were conducted using four normal load levels (F_N) and eight scratching directions (ϕ) to evaluate the existence of anisotropic behavior. A data processing approach based-on linear and non-linear mathematical models enabled the description of the experimental results, allowing both the identification and quantification of friction anisotropy, as

* Corresponding authors.
E-mail addresses: guilherme.bernardes@femto-st.fr (G.B. Rodrigues), guillaume.colas@femto-st.fr (G. Colas).

https://doi.org/10.1016/j.triboint.2026.111721
Received 27 October 2025; Received in revised form 7 January 2026; Accepted 17 January 2026
Available online 23 January 2026

well as the characterization of its symmetry properties. To ensure the reliability of the results, an uncertainty traceability assessment was performed, guaranteeing a 95 % confidence level in all analyses. Finally, post-scratch investigations established correlations between the frictional response and morphological characteristics, similar to those previously observed in tungsten films [10]. However, particular attention is given to one specific film that exhibits an atypical behavior.

2. Materials and method

A in-house designed DC magnetron sputtering system was used to deposit molybdenum films on silicon (100) substrates with a thickness of 525 μm and a surface area of 20 × 10 mm^2. Prior to deposition, the substrates were ultrasonically cleaned in acetone and ethanol for 10 min and subsequently dried using a N_2 flux. A high-purity molybdenum target (99.9 %) with a diameter of 51 mm was positioned 65 mm away from the substrate inside a vacuum chamber with a residual vacuum of approximately 10^{-5} Pa. The substrates were tilted at eight different deposition angles, α = 0°, 30°, 40°, 50°, 60°, 70°, 80°, and 85°. For all deposition conditions, the target current was maintained at 200 mA, while an argon flow rate of 2.6 sccm was used, resulting in a sputtering pressure of approximately 2.8 × 10^{-1} Pa. A thickness calibration was carried out to adjust the deposition time, ensuring that the resulting Mo films had an average thickness of 520 ± 50 nm. After deposition, the films were carefully wrapped in wipe paper, placed in an acrylic box, and stored in a vacuum-sealed bag under low vacuum to prevent contamination. The films were stored for one week before scratching tests and characterization.

Morphological characterization of all films was carried out using a Thermofisher Apreo S low-vacuum Scanning Electronic Microscope (SEM), analyzing both top and cross-section images. Film thickness (t) was measured using a Bruker Dektak XT profilometer equipped with a 12.5 μm radius tip and a 45° cone angle. Nine thickness measurements were taken, uniformly distributed across both extremities, to assess potential variations along the sample length. Additionally, the films were cleaved using a diamond pen, ensuring that the film integrity was maintained during the process, and the inclination of the film structures relative to the substrate normal (β) was determined. Ten independent measurements on different cross-section views of each film were performed.

Grazing-incidence X-ray diffraction (GIXRD) analyses were performed using a Malvern Panalytical Aeris diffractometer with Cu-Kα radiation (λ = 1.5418 Å), operated at 30 kV and 10 mA. Measurements were collected at a fixed incidence angle of 0.8°, within a 2θ range between 20° and 90°. To evaluate whether the Mo grains exhibited preferred orientations, pole figure measurements were conducted using a Bruker D8 Discover AXS diffractometer in θ/θ geometry with a parallel beam and a Co-Kα source. In this analysis, the first two diffraction planes observed in the GIXRD patterns, (110) and (200), were examined. The sample surface normal angle (Ω) varied from 0° to 360°, while the tilt angle (χ, measured relative to the vertical axis) ranged from 0° to 80°, both with a step size of 1°. The TEXEVAL software from Bruker AXS was used to apply defocalisation corrections and generate the pole figure representations.

2.1. Scratching tests

An Anton Paar GmbH Micro Scratch MST3 equipped with a custom sample holder was used to perform scratch tests at constant normal force. A spheroconical Rockwell diamond tip indenter (100 μm radius, 120° conic angle) was used. Four different normal load values (F_N) were selected: 1.50 N, 2.50 N, 3.25 N, and 4.00 N, corresponding to contact pressures between 7.2 and 18.3 GPa, estimated using the model proposed by Liu et *al.* [18]. These normal loads were carefully selected to avoid any degradation of the films.

Each scratch test was conducted over a 0.5 mm single scratch length at a sliding speed of 6 mm/min under controlled room conditions (relative humidity: 47 ± 2 %, temperature: 22.0 ± 0.6 °C). This scratch length corresponds to approximately eight times the contact diameter, ensuring effective pure sliding over the entire contact. The normal force and the projection of tangential force at the scratching direction (F_N and F_T, respectively) were recorded using sensors with 6 mN resolution. Three repetitions were performed for each condition, followed by a verification of the Coulomb's law [19]. In line with the previous study [10], average F_T/F_N values were calculated over a stable portion of the curves, and if these values were statistically equivalent for all applied F_N, a Coulomb-type frictional response was confirmed, defining the friction coefficient as $\mu = F_T/F_N$.

For non-zero deposition angles ($\alpha \neq 0°$), the films exhibit a tilted structure, even when a well-defined columnar formation occurs. This tilt is oriented toward the incident atom flux direction. To assess anisotropic frictional behavior, we defined scratching directions based on this structural inclination. Scratching along the tilt direction was assigned $\phi = 0°$, while the opposite direction was defined as $\phi = 180°$, as shown in Fig. 1(a). Six additional directions were established by rotating counterclockwise in 45° increments (Fig. 1(b)). The set of tests previously described was conducted for each of these eight ϕ values to systematically evaluate the influence of film orientation on frictional behavior. Moreover, an uncertainty traceability assessment, similar to that used in our previous study [10], was performed, ensuring a 95 % confidence level for all results.

2.2. Friction anisotropy

A linear model, similar to the one employed in the previous study [10], is applied here to describe friction anisotropy. This model is grounded in the formulation proposed in [20,21], which extends Coulomb's law to a sliding regime, where the sliding direction is denoted by the vector $\underline{v} = \begin{bmatrix}\cos(\phi)\\ \sin(\phi)\end{bmatrix}$. The model assumes a linear relationship for the friction force, $f(\underline{v})$, as a function of $\underline{v}$, expressed as $f(\underline{v}) = |F_N|\, C \cdot \underline{v}$, where C is a second-order tensor in $\mathbb{R}^2$. As suggested by Rodrigues et *al.* [10], although the tensor C may exhibit an asymmetric component, only its symmetric part, $\tilde{C}$, is probed during scratch testing. Consequently, a Singular Value Decomposition (SVD) of this symmetric component is employed to describe the directional dependence of the friction coefficient $\mu(\phi)$.

$$\begin{bmatrix}C_{11} & C_{12}\\ C_{12} & C_{22}\end{bmatrix} = \tilde{C} = \mathcal{U} \cdot \mathcal{G} \cdot \mathcal{U}^t = \begin{bmatrix}\cos(\gamma) & -\sin\gamma\\ \sin\gamma & \cos(\gamma)\end{bmatrix}\begin{bmatrix}g_1 & 0\\ 0 & g_2\end{bmatrix} \times \begin{bmatrix}\cos(\gamma) & -\sin(\gamma)\\ \sin(\gamma) & \cos(\gamma)\end{bmatrix}^t \quad (1)$$

$$\mu(\phi) = C_{11}\cos^2\phi + 2C_{12}\cos\phi\sin\phi + C_{22}\sin^2\phi \quad (2)$$

A least-squares approach is used to fit with the linear model, which can be expressed using three parameters, either in the form of (C_{11}, C_{12}, C_{22}) or, equivalently, as (γ, g_1, g_2). As the experimental data allow evaluation in eight ϕ directions, an overdetermined system is obtained. Following the approach of [10], the parameters g_1 and g_2 are obtained, and the normalized anisotropy degree is defined as $\overline{\Delta g} = 2(g_1 - g_2)/(g_1 + g_2)$. This scalar parameter quantitatively describes the degree of friction anisotropy, where an isotropic response corresponds to $\overline{\Delta g} = 0$.

Furthermore, the deviation between the linear model fit and the experimental data is evaluated using $\underline{R} = \mathcal{M} \cdot \underline{C}_{lsq} - \underline{\mu}$. $\mathcal{M}$ is the matrix such that $\mathcal{M}_{i1} = \cos^2\phi_i$, $\mathcal{M}_{i2} = 2\cos\phi_i \sin\phi_i$ and $\mathcal{M}_{i3} = \sin^2\phi_i$, and $\underline{C}_{lsq}$ is the tensor containing the least-squares solution. $\underline{R}$ is then applied to calculate the normalized residual $\eta = \sqrt{\frac{\underline{R}^t\underline{R}}{\underline{\mu}^t\underline{\mu}}}$.

This linear formulation inherently leads to centrosymmetric fitting curves, as noted by [22], which means that it cannot describe

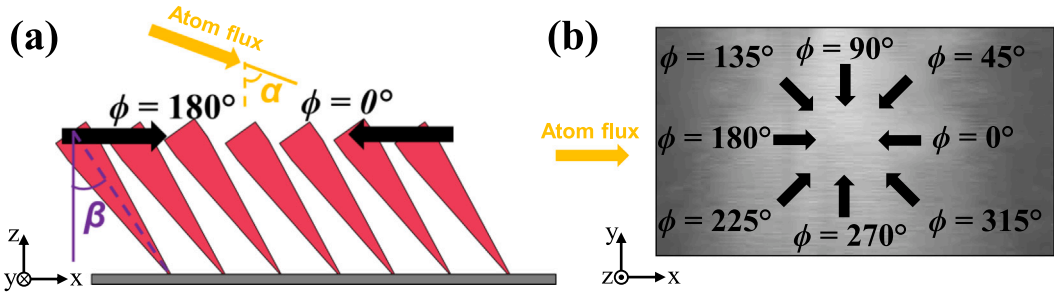

Fig. 1. (a) A schematic illustration shows the deposition angle, α, which results in a directional columnar growth aligned with the molybdenum atom flux. This column tilt serves as a reference to define the scratching directions: $\phi = 0°$ corresponds to scratching along the tilt direction, while $\phi = 180°$ corresponds to scratching against it. (b) All eight ϕ directions are established by rotating counterclockwise in 45° increments.

differences between opposite directions. To address this limitation, a non-linear model is introduced in this work by incorporating a third-order tensor, $\mathcal{T}$, enabling the representation of non-centrosymmetric behavior. In addition to the previous linear function,

$$f\left(\underline{v}\right) = \left(C \cdot \underline{v} + \mathcal{T} : \underline{v}\underline{v}\right)\left|F_N\right| \tag{3}$$

As for the linear model, when a scratch tester is used, only the projection of the friction force along the scratching direction $\underline{v}$ is measured. Thus, only the symmetric part of $\mathcal{T}$, the tensor $\mathcal{H}$, is assessed. This tensor is fully symmetric and thus depends on four parameters such as: $\mathcal{H}_{111}$, $\mathcal{H}_{112} = \mathcal{H}_{121} = \mathcal{H}_{211}$, $\mathcal{H}_{122} = \mathcal{H}_{212} = \mathcal{H}_{221}$ and $\mathcal{H}_{222}$.

Following the same procedure as for the linear model, a projection is carried out using the least-squares method, now incorporating the four parameters defined for $\mathcal{H}$. These parameters play a key role in determining the curves non-centrosymmetry. The norm of $\mathcal{H}$, denoted as $\|\mathcal{H}\|$, quantifies the extent of non-linearity in the model.

2.3. Post-scratch investigations

Focused Ion Beam (FIB) cross-sections were performed at the center of the scratches using a Zeiss Ultra 55 SEM-FEG FIB to conduct post-scratch investigations. Procedures were carried out at 30 keV, with a protective platinum layer applied prior to surface etching, followed by a cleaning procedure for the cross-sections. They were then examined using Scanning Electron Microscopy (SEM). Given the expected variation in thickness for the films, especially those deposited at higher α angles, FIB zones were selected in close proximity, within regions of similar thickness.

3. Results and discussion

3.1. As-deposited Mo films

Table 1 shows the film thickness, column tilt angle (β), and growth rate for all the considered films. As α increases, the corresponding β values also increase. Although a clear relationship between α and β is observed, it appears non-linear. However, none of the models reported in literature [23,24] may be directly applied to the present results. This is expected, as β is known to depend on various empirical factors, including material and sputtering pressure [9,25–27].

Fig. 2 shows both surface and cross-sectional views of Mo films deposited at $\alpha = 0°$, 40°, 50° and 85°, with the yellow arrow indicating the direction of the atom flux during deposition (see Section 1 of supplementary information for all films). Cross-section views confirm the presence of a columnar structure for all α angles, along with notable variations in film porosity and morphology. Films deposited at $\alpha = 0°$ and 30° exhibit a dense and compact structure, despite the columnar growth. In these cases, the atoms possess sufficient energy to promote the coalescence of the individual structures during GLAD deposition.

Fig. 3(c) and (d) show that above $\alpha = 40°$, the morphology changes considerably. Although the structure remains relatively dense,

Table 1
Summary of molybdenum films deposited by GLAD at various deposition angles.

Deposition angle, α (°)	Deposition time	Thickness (nm)	Growth rate (nm/h)	Column angle, β (°)
0	17′15″	484 ± 6	1648 ± 21	0.8 ± 0.9
30	19′40″	486 ± 21	1482 ± 64	12.3 ± 3.1
40	21′48″	546 ± 28	1502 ± 77	21.4 ± 3.1
50	24′45″	570 ± 12	1382 ± 29	26.3 ± 1.7
60	28′35″	568 ± 17	1192 ± 36	29.7 ± 1.3
70	37′46″	558 ± 39	886 ± 62	34.5 ± 2.2
80	56′30″	495 ± 31	525 ± 33	38.1 ± 1.3
85	78′43″	502 ± 50	383 ± 38	42.1 ± 1.3

the columns appear randomly oriented, and no consistent column apex shape is observed. When α reaches 50°, a significant increase in porosity is observed, with column apexes becoming more elongated in the direction perpendicular to the atom flux, which corresponds to $\phi = 90°/270°$. Beyond $\alpha = 50°$, increasing the deposition angle results in higher porosity and even more pronounced column elongation. This morphological evolution is typically observed for GLAD films of different materials. It has been closely associated to the shadowing effect [26,28–32]. This phenomenon results directly from the geometrical configuration of GLAD deposition [9], and this range of deposition angles is cited as critical for $\alpha \leq 60°$ [33]. That was confirmed in our recent study on W films [10]. However, in contrast to this observation, the Mo films investigated herein exhibit significant morphological changes due to the shadowing effect starting from $\alpha = 50°$.

Considering that identical deposition parameters were applied to both Mo and W films, this difference can reasonably be attributed to intrinsic material properties, such as the lower atomic mass of Mo compared to W, which enhances surface mobility and allows them to diffuse toward less-shadowed regions. As a result, at larger α angles, a more pronounced fanning effect is observed, characterized by highly elongated columns oriented perpendicular to the atom flux. This leads to a "worm-shaped" aspect of the column tops, as observed for the red-highlighted column in Fig. 2(g).

Fig. 3 presents the XRD patterns for the Mo films, with diffraction peaks corresponding to Bragg reflection planes (110), (200), (211) and (222), all of which are associated with the body-centered cubic (bcc) Mo phase. This observation is consistent with reports in the literature [34–39]. According to Liedtke et al. [36], the (110) plane is thermodynamically favored due to its lowest surface energy. However, as α increases, the number of atoms arriving at the substrate with trajectories favorable to forming this plane may decrease, potentially leading to the development of a bi-axial texture [34].

This behavior has been reported in previous studies of Mo films deposited at angles $\alpha = 30°$, 45°, 60°, 85° [13]. In agreement with these findings, the present study also shows that the (110) reflection remains the most intense across all films. Nevertheless, a marked

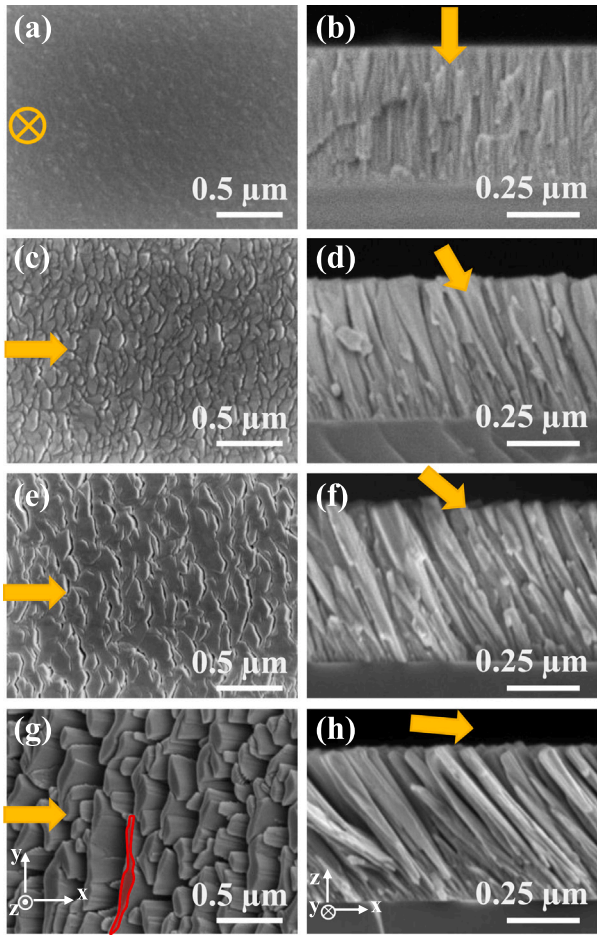

Fig. 2. Surface and cross-section views by SEM of molybdenum films deposited at different deposition angles. (a)–(b) $\alpha = 0°$, (c)–(d) $\alpha = 40°$, (e)–(f) $\alpha = 50°$ and (g)–(h) $\alpha = 85°$. The yellow arrows indicate the direction of the molybdenum atom flux during GLAD deposition.

reduction in peak intensity is observed at the largest α values (80° and 85°), indicating a possible shift in preferred orientation and potential reduction of the crystal size at extreme obliqueness. This is confirmed by the fact that the (211) plane started to be more present. This change may be attributed to the increasing dominance of shadowing effect at higher deposition angles, which tilts the crystallographic orientation away from direction perpendicular to the substrate surface. At lower angles, some degree of recrystallization and surface mobility may occur, resulting in fewer changes in orientation [34].

Fig. 4(a) and (b) present the (110) pole figures for the films deposited at $\alpha = 0°$ and 80°, respectively. Since the (110) plane is energetically favored in Mo thin films [36], a growth orientation along this plane is expected for perpendicular deposition ($\alpha = 0°$). This is confirmed by the centered distribution observed in the (110) pole figure of the film deposited at $\alpha = 0°$ (Fig. 4(a)), indicating that the (110) planes lie parallel to the substrate. A similar result was reported by Chen et al. [13] for Mo films deposited at normal incidence, attributing this configuration to the interfacial energy minimization that promotes (110) orientation, even in the absence of grain recrystallization.

The film deposited at $\alpha = 80°$ exhibits one pole centered at approximately $\chi = 28°$ and two additional poles around $\chi = 35°$. This suggests that the (110) planes are inclined at an angle close to β, which was measured to be 38.1° ± 1.3°. Moreover, considering that the angle between the (110) and (111) planes in a bcc is about 35.3°, it can be inferred that the (111) plane lies approximately parallel to the substrate surface, as illustrated in Fig. 4(b).

For the film deposited at $\alpha = 40°$ (Fig. 5(a) and (b)), the pole figures for the (110) and (200) planes show a different behavior. Two distinct grain orientations are identified within the (110) plane family, appearing at inclination angles of $\chi = 20°$ and $\chi = 12°$, which correspond to the (110) and (–110) planes, respectively. The first group exhibits a crystallographic orientation where the (110) planes are inclined by a value that closely matches the measured column tilt angle β of this film (21.4° ± 3.1°). The second group displays a tilt of approximately 12° with respect to the substrate normal. This is corroborated by the (200) pole figure, which shows a pole at $\chi = 33°$. The sum of these angles, 33° +12° = 45°, is consistent with the known angular separation between the (110) and (200) planes, as illustrated in Fig. 5(c). However, contrary to the pole figures of films deposited at $\alpha = 0°$ and 80°, the azimuthal positions of the poles for the film deposited at $\alpha = 40°$, are located at approximately $\Omega \approx 65°$ and 245°, indicating that the (110) planes are inclined relative to the direction of the incident Mo atom flux.

3.2. Friction behavior

A preliminary analysis was conducted to compare the friction responses at different F_N (1.50 N, 2.50 N, 3.25 N, and 4.00 N) for all α angles and ϕ directions. Fig. 6 presents the F_T/F_N average values *vs.* scratching directions curves, for Mo films deposited at $\alpha = 0°$, 40°, and 85°. Each symbol marker denotes the average F_T/F_N value obtained from scratch tests, while the solid lines represent the fit curves based on the linear model. For films deposited at $\alpha = 0°$ and 85°, the curves corresponding to different F_N values largely overlap, indicating that the friction response remains independent on the applied normal load. This behavior suggests that these films adhere to Coulomb's law, thus $\mu = F_T/F_N$. A similar trend was observed for all films, with the exception of the film deposited at $\alpha = 40°$. As it can be seen in Fig. 6, the data points deviate from the linear fit and, for a given normal force, require the non-linear model for accurate fitting. Furthermore, at $\alpha = 40°$, the F_T/F_N value increases with higher F_N, particularly in the directions $\phi = 0°$, 45°, and 315°, indicating a deviation from Coulomb's law behavior and a non-centrosymmetry.

We thus distinguished films with Coulombic and non-Coulombic friction behaviors in the following.

3.2.1. Mo films with Coulomb's frictional behavior

Fig. 7 presents the $\mu(\phi)$ polar plots obtained from the scratching tests performed at $F_N = 3.25$ N on the Mo films that follow Coulomb's law. The dotted lines represent the 95 % confidence intervals for the friction coefficient values. A first observation is that, under the conditions applied in this study, the friction coefficients of all films remain relatively low for dry friction, with values of $\mu(\phi) \leq 0.06$. The films are then grouped according to the shape and symmetry of their curves, as well as their $\overline{\Delta g}$ (Fig. 8) and residuals values (Fig. 9). The classification terminology applied here is consistent with that used in our previous study [10].

1. $\alpha = 0°$: Isotropic behavior confirmed by circular shaped curve, lower residuals and lower $\overline{\Delta g}$ values.
2. $\alpha = 30°$: Despite exhibiting a nearly circular shape curve, low residuals, and a small $\overline{\Delta g}$ value, a statistically significant difference in friction coefficient (μ) is observed between the directions $\phi = 0°$ and 180°. This indicates a slight non-centrosymmetric anisotropy in the tribological response of the film.
3. $50° \leq \alpha \leq 85°$: Although variations in μ levels, curve shapes, and $\overline{\Delta g}$ values, all films within this range exhibit orthotropic behavior. This is characterized by the distinctive "peanut-shaped" $\mu(\phi)$ curves: Lower μ values occur at $\phi = 0°$ and 180°, intermediate values at $\phi = 45°$, 135°, 225°, and 315°, and the highest values at $\phi = 90°$ and 270°. The film deposited at $\alpha = 50°$ presents the most pronounced anisotropy, with $\overline{\Delta g} = 0.72 \pm 0.06$, which

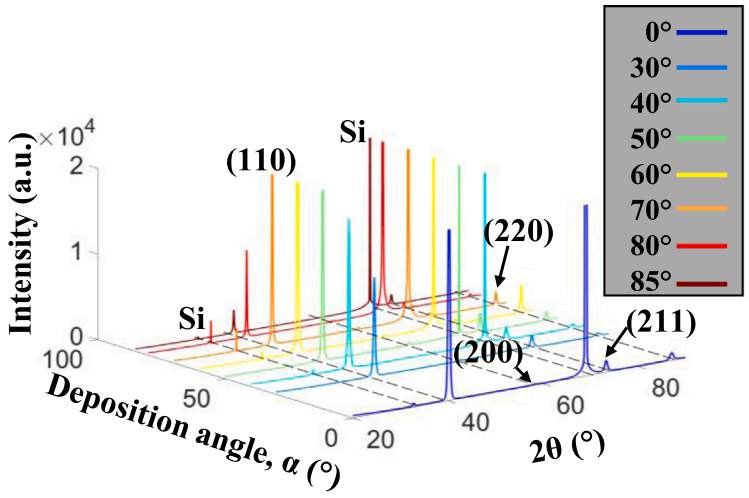

Fig. 3. XRD patterns of molybdenum films deposited at various deposition angles. Silicon and body-centered cubic (bcc) Mo phase are identified.

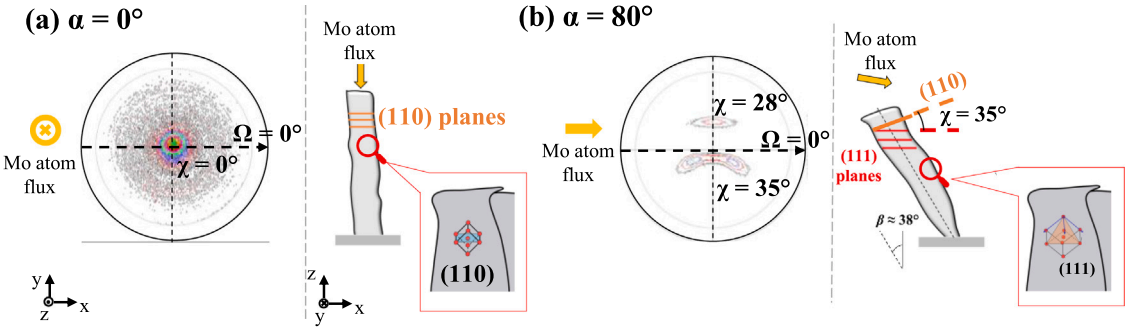

Fig. 4. Pole figures and schematic representations of the preferred grain orientations for Mo films deposited at (a) $\alpha = 0°$ and (b) $\alpha = 80°$. Yellow arrows indicate the direction of the Mo atom flux during deposition.

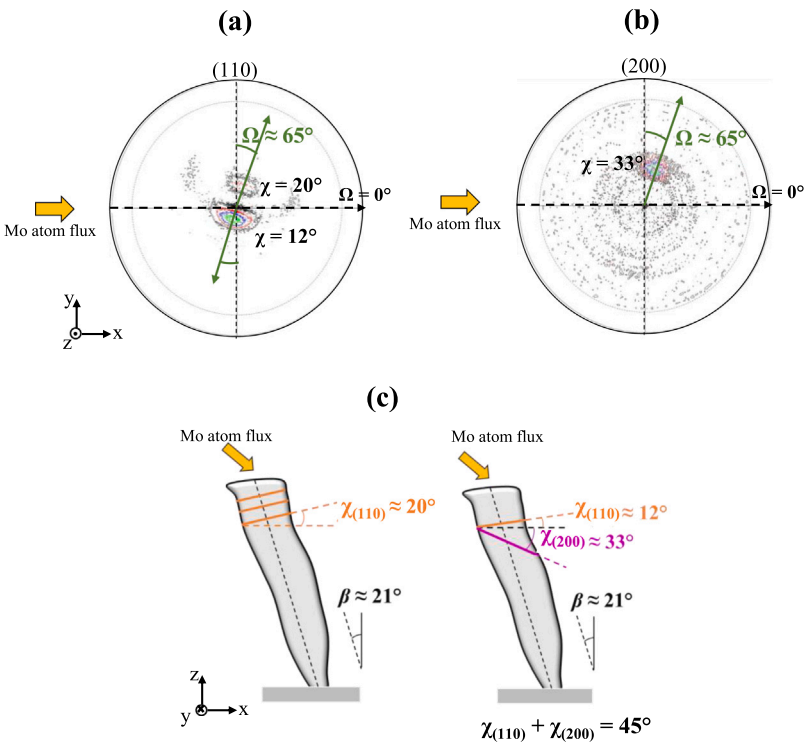

Fig. 5. Pole figures of (a) (110) and (b) (200) planes of the Mo film deposited at $\alpha = 40°$, as well as (c) schemes representing preferred orientation of the two grain groups in a column. The yellow arrows indicate the Mo atom flux.

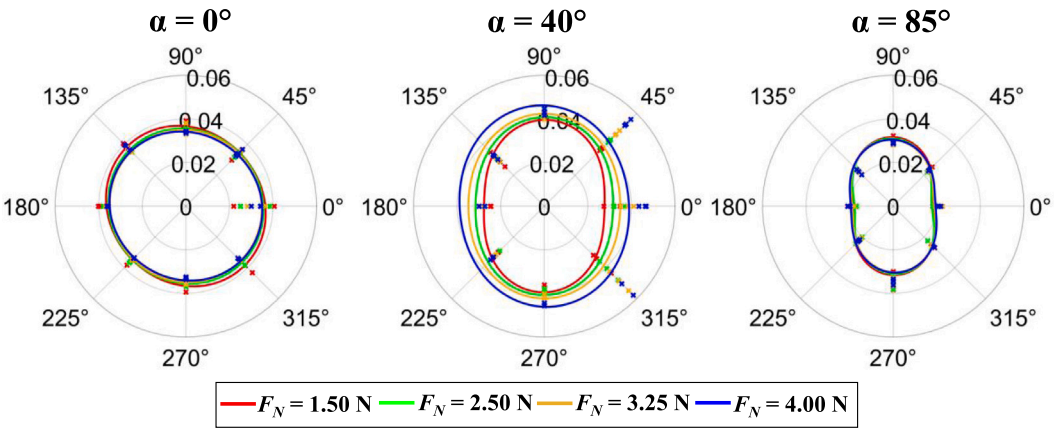

Fig. 6. Results for the Mo films deposited at α = 0°, 40° and 85°. The friction coefficients (μ) obtained for each normal load (F_N) are evaluated for all scratching directions (ϕ).

gradually decreases to $\overline{\Delta g}$ = 0.47 ± 0.07 for the film deposited at α = 85°. Moreover, a notable reduction in overall μ levels is observed: From approximately 0.05 in the ϕ = 90°/270° directions for α = 50°, down to 0.03 for the same directions at α = 85°.

Furthermore, some films exhibit slightly non-centrosymmetric responses in μ values between specific scratching directions: (i) For films deposited at α = 50° and 80°, differences are observed between the ϕ = 90° and 270° directions, and (ii) for the film deposited at α = 60°, a discrepancy is evident between the ϕ = 0° and 180° directions. Finally, the inclination of the fitting curves, defined by the parameter γ, is close to 90° for all films, which confirms the presence of strong orthotropy associated to the columns preferred orientation.

Similarly to W films [10], in contrast to what is generally suggested in the literature [11,40–43], the dominant friction anisotropy observed in the Mo films investigated in this study, under the applied contact conditions, is orthotropic. This anisotropy is even more pronounced than that reported for W films [10], as evidenced by the higher $\overline{\Delta g}$ values observed herein. The other slight anisotropies observed, either between ϕ = 0° and 180°, or between ϕ = 90° and 270°, are far less prominent, with differences close to uncertainty intervals. Despite minor variations in the crystallographic characteristics revealed by XRD patterns and the presence of preferred grain orientations shown in the pole figures, no direct correlation was found between crystallography and frictional behavior. Instead, the primary factor governing the presence or absence of friction anisotropy is the film morphology.

The film deposited at α = 0°, due to its dense and fibrous morphology, responds as a bulk film, i.e., isotropic. For the film deposited at α = 30°, the possible explanation for its slight non-centrosymmetric behavior is double. Firstly, as suggested by the literature [11,40–43], the columns tilt pointing towards the atom flux induces an anisotropy between ϕ = 0° and 180°. However, upon closer observations, the surface of this film presents overlapping columns, forming a "fish scale" aspect that may have influenced the frictional response (Fig. 10). Some authors have suggested that not only mechanical, but also frictional anisotropy can be obtained by using similar bio-inspired "fish scale" features on surfaces [44–47].

For the films deposited at 50° ≤ α ≤ 85°, the morphological influence arises from a combination of column top geometry and the variation in intercolumn voids volume. As suggested in a previous study [10], the preferential elongation of column tops in the direction perpendicular to the incident atom flux, corresponding to ϕ = 90° and 270°, results in distinct deformation modes within the film. The presence of elliptical column structures, as observed in Mo films deposited within this α range, promotes the formation of so-called "chain columns". This phenomenon has been reported as a key factor contributing to the anisotropic behavior of various physical properties in GLAD films [31,48–50].

Fig. 11 illustrates that when the indenter scratches along the directions ϕ = 0° and 180°, the columnar structures exhibit greater deformation due to the higher porosity aligned with these orientations. In these directions, the intercolumn voids allow the individual columns to bend and lean onto adjacent ones, and under the severe contact conditions applied in this study, undergoing plastic deformation (Fig. 11(a)). In contrast, when scratching occurs along ϕ = 90° and 270°, the columns are more closely packed, leading to earlier mechanical interaction with neighboring columns. This restricts the extent of plastic deformation, resulting in increased reaction forces and, consequently, higher friction coefficients (Fig. 11(b)).

This behavior is consistent with the post-scratch analysis of W films from our previous study [10], where distinct deformation modes were observed when scratching along the ϕ = 0° and 90° directions. In that study, a 1D mechanical model proposed provides an analytical support for the role of plastic deformation as a factor responsible for reducing the friction coefficient at directions ϕ = 0° and 180°. In fact, scratching along the ϕ = 90° and 270° directions leads to a larger column–column contact amount, which reduces deformation. As a result, the film offers greater resistance to the indenter, and consequently, higher friction coefficients are observed in these directions.

However, a notable distinction from the W film results [10] is the overall decrease in both the friction coefficient (μ) and the anisotropy degree ($\overline{\Delta g}$) across the range 50° ≤ α ≤ 85° (Figs. 7 and 9). For W films exhibiting orthotropic behavior, the only sample with a lower $\overline{\Delta g}$ was that deposited at α = 60° (0.26 ± 0.02), whereas films deposited at 70° ≤ α ≤ 85° showed statistically equivalent values of approximately 0.35. These values are considerably smaller, and no reduction trend was observed compared with those obtained in the present study for α ≥ 50°. A plausible explanation for this behavior lies in the increased volume of intercolumnar voids in the Mo films, which may reduce the directional dependence of deformation and friction by promoting a more homogeneous mechanical response across different scratch orientations.

Fig. 12 presents FIB cross-sections of the Mo films deposited at α = 60° and 80°, highlighting three distinct zones: The as-deposited region and two regions submitted to scratching at ϕ = 0° and ϕ = 90°. For the film deposited at α = 60°, only a modest reduction in overall film thickness is observed, with the region scratched at ϕ = 0° exhibiting more pronounced deformation. In contrast, the region scratched at ϕ = 90° shows columns that appear more separated and that retain a morphology closer to that of the as-deposited structure. Additionally, columns in the region scratched at ϕ = 0° show a higher degree of inclination relative to the substrate normal after scratching (β' = 42.1°

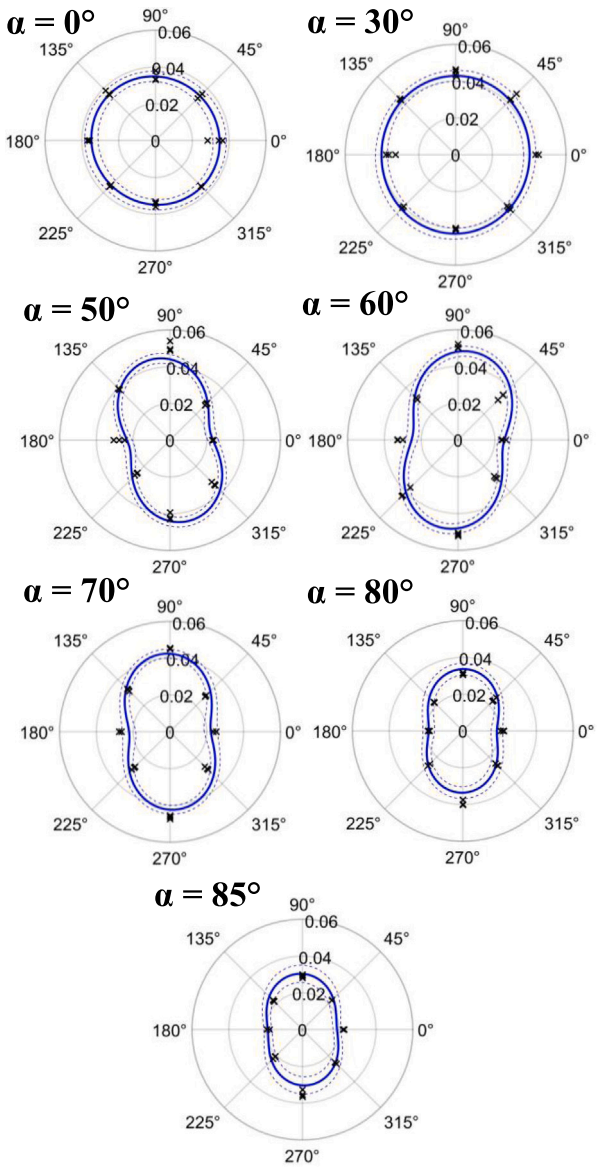

Fig. 7. Friction coefficients as a function of scratching directions, $\mu(\phi)$, for Mo films with Coulomb's frictional response deposited at various deposition angles, α, with F_N = 3.25 N. The symbols represent the experimental data. The solid line is the fit obtained via the linear model, and the dotted lines represent the 95 % confidence interval.

± 2.3°) compared to those scratched at ϕ = 90° (β' = 33.8° ± 3.0°), indicating greater plastic deformation. Interestingly, the post-scratch column inclination at ϕ = 90° is statistically comparable to the β angle measured for the as-deposited film at α = 60° (β = 29.7° ± 1.3°), suggesting that scratching along this directions leads to lower plastic deformation. These inclination angles were determined by averaging 10 measurements based-on the main axis orientation of the columns.

For the Mo film deposited at α = 80°, distinct deformation behaviors are observed between the scratching directions ϕ = 0° and 90°, due to the column-chain effect. A pronounced degree of plastic deformation is evident, as indicated by a reduction of approximately 130 nm in film thickness when comparing the as-deposited and scratched regions. This reduction is notably greater than that observed for the film deposited at α = 60°, which can be attributed to the greater amount of intercolumn voids present in the α = 80° film. Despite the increased porosity, no significant difference in thickness is observed between the regions

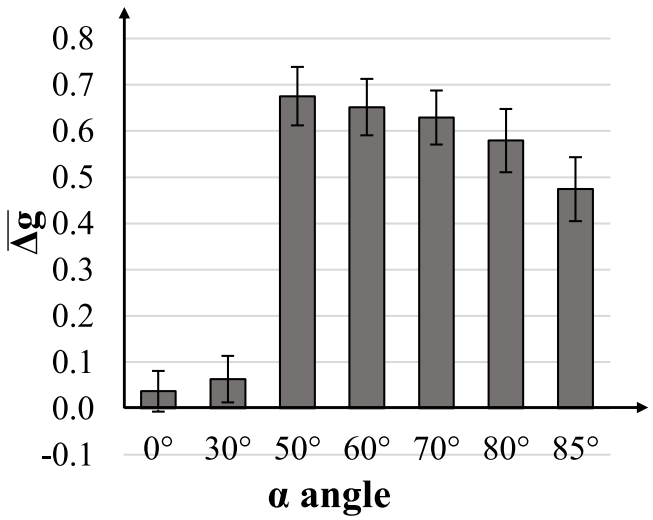

Fig. 8. Anisotropy degree, $\overline{\Delta g}$, obtained using the linear model parameters for all molybdenum films with Coulomb's frictional behavior deposited at different deposition angles (α) and scratched with normal load F_N = 3.25 N.

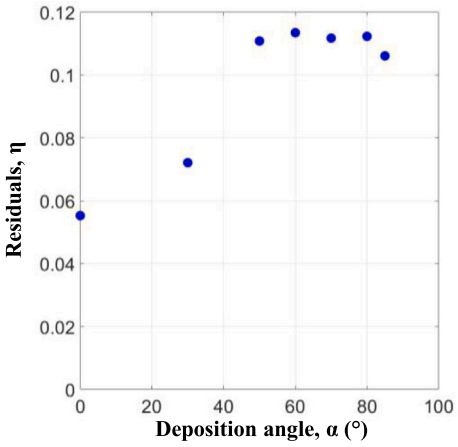

Fig. 9. Residuals (η) of the linear model for the $\mu(\phi)$ curves of molybdenum films with Coulomb's frictional behavior and scratched with normal load F_N = 3.25 N.

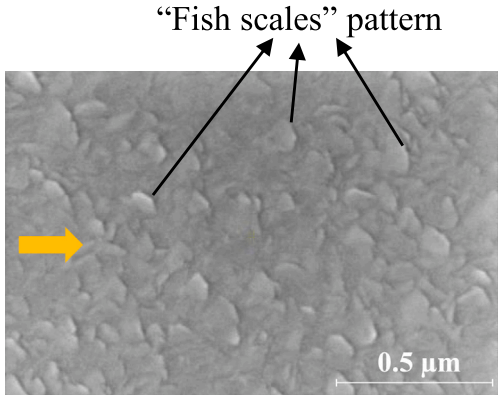

Fig. 10. A surface view of the Mo film deposited at α = 30°, exhibiting in detail the presence of a "fish scale" pattern in the direction of the flux atom, indicated by the yellow arrow.

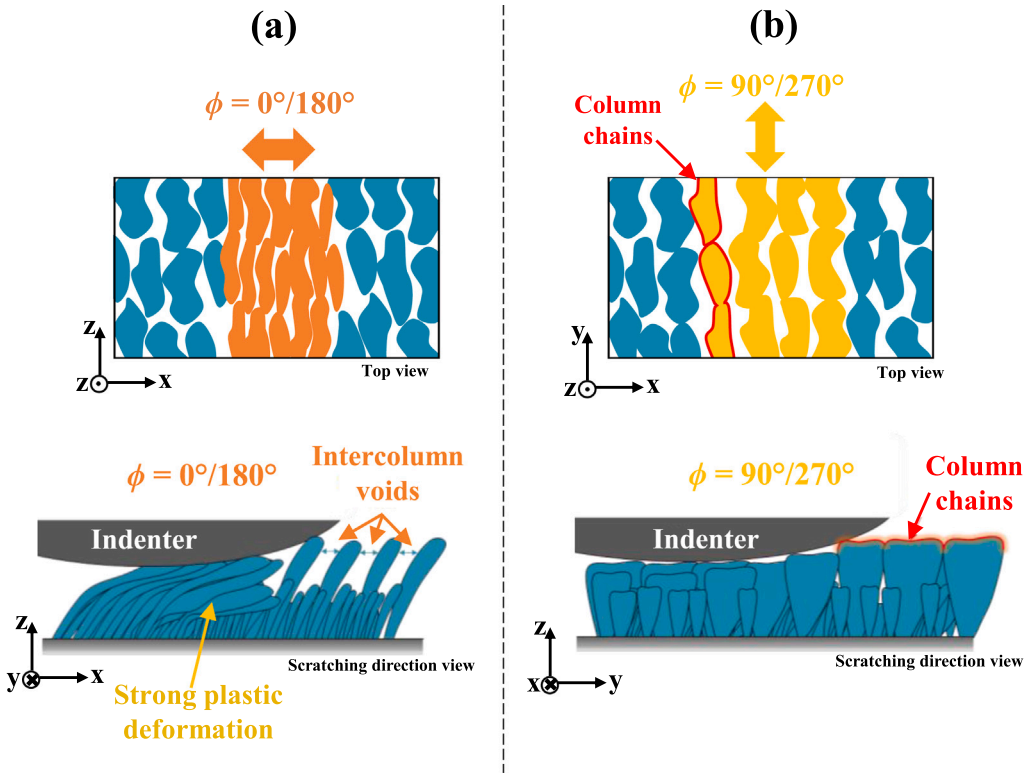

Fig. 11. Schemes of top and scratching directions views summarizing mechanisms associated with the friction anisotropic behavior for Mo films scratched along (a) $\phi = 0°$ and 180° directions, and (b) $\phi = 90°$ and 270°.

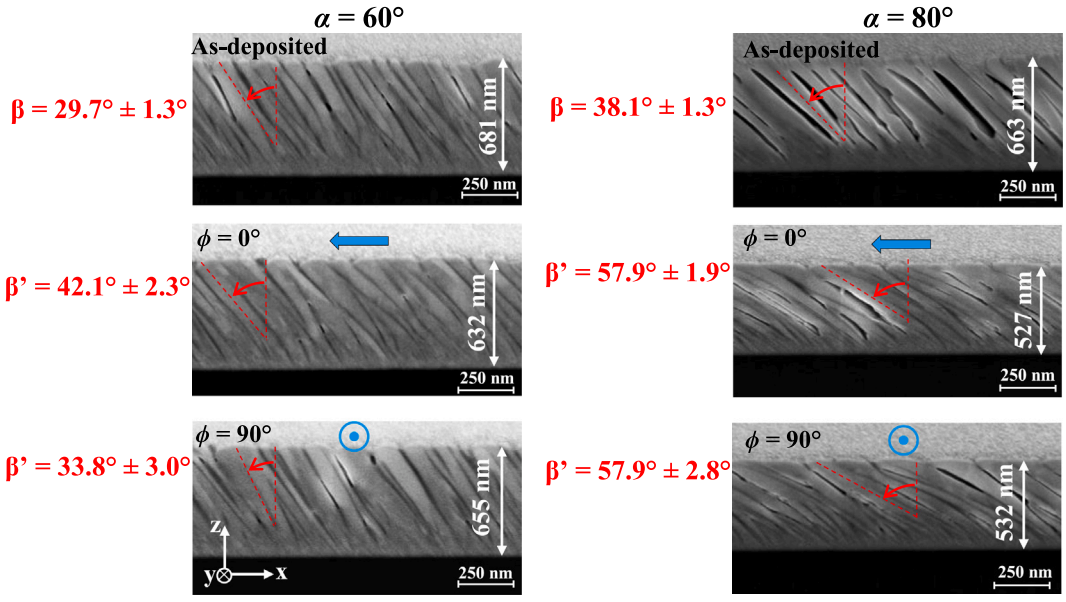

Fig. 12. FIB cross-section views of Mo films deposited at $\alpha = 60°$ and 80°, in an as-deposited and scratched zones at $\phi = 0°$ and 90°. These scratching direction are indicated by the blue arrows.

scratched at $\phi = 0°$ and 90°, in contrast to the behavior of the $\alpha = 60°$ film. This suggests that the highly porous structure of the $\alpha = 80°$ film may facilitate more uniform deformation across different directions.

As previously discussed and further evidenced by the FIB cross-sections, it is clear that the void amount increases substantially with increasing α, accompanied by a morphological evolution of the columns into a "worm-shaped" structure. This transition results in a significant rise in overall porosity. At high α values, the porosity becomes so pronounced that it appears to reduce the effectiveness of the "column-chain" effect, thereby contributing to a decrease in the degree of anisotropy. Furthermore, this extensive porosity may also account for the overall reduction in friction coefficient (μ) levels, as less

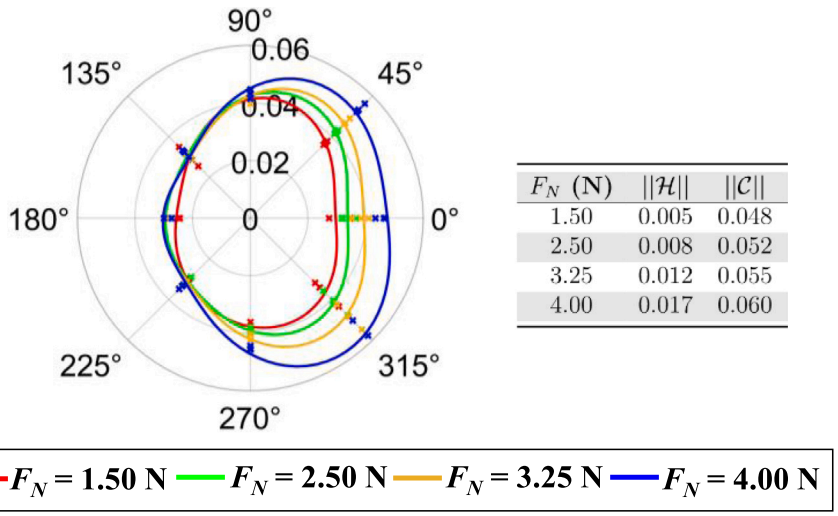

F_N (N)	$\|\|\mathcal{H}\|\|$	$\|\|\mathcal{C}\|\|$
1.50	0.005	0.048
2.50	0.008	0.052
3.25	0.012	0.055
4.00	0.017	0.060

Fig. 13. Friction coefficient as a function of scratching directions ($\mu(\phi)$) curves for the film deposited at $\alpha = 40°$ scratched with the four normal loads F_N, and fitted using the non-linear approach. The $\|\mathcal{H}\|$ and $\|C\|$ values obtained by the non-linear model are presented for each F_N.

intercolumnar interactions across all scratching directions are present, which may reduce lower friction forces during scratch. This behavior can be explained by the 1D mechanical model proposed in a previous study [10] by including a slight modification. In that model, it is assumed that the second accommodation mechanism develops along a characteristic distance p, which may be defined based on morphology as the distance between adjacent columns. A potential way to improve this approach could involve modifying these limit conditions by introducing additional variables that account for other morphological features, such as column shape and inter-column interactions.

The slight anisotropies observed for films deposited at $\alpha = 50°$, 60°, and 80° remain an open question. A plausible explanation may lie in the morphological characteristics of the films. It is possible that features such as the tilt of the columnar axes and the concave geometry of the column tops, curved toward the direction of the incoming atom flux, may introduce asymmetries. These morphological asymmetries could influence the mechanical response during scratching, thereby contributing to the observed subtle anisotropic friction behavior.

3.2.2. *Mo film deposited at $\alpha = 40°$*

As previously mentioned, the Mo film deposited at $\alpha = 40°$ does not strictly adhere to Coulomb's law and exhibits a non-centrosymmetry, which necessitates a complementary approach beyond the linear model. Fig. 13 thus presents the $\mu(\phi)$ polar plots for the Mo film deposited at $\alpha = 40°$, and obtained using the non-linear model. A substantial improvement in the fitting accuracy is observed compared to the results obtained using the linear model (to see Fig. 6). Notably, the residual for the curve corresponding to $F_N = 4$ N decreases from 0.23 to 0.08, highlighting the enhanced capability of the non-linear model to more accurately capture the experimental friction behavior under this deposition condition.

In the $\mu(\phi)$ curves for the film deposited at $\alpha = 40°$, a pronounced asymmetry is observed relative to the 90°/270° axis, while a notable symmetry is maintained with respect to the 0°/180° axis, particularly at higher F_N values. These results further emphasize the non-Coulombic behavior of the film, characterized by a frictional response that is strongly dependent on the applied normal load. Additionally, significant differences are observed between the following opposing directions: $\phi = 0°$ and 180°, $\phi = 45°$ and 315°, and $\phi = 225°$ and 135°. Interestingly, the only directions exhibiting statistically similar μ values are $\phi = 90°$ and 270°.

As previously discussed, the norm $\|\mathcal{H}\|$ provides a quantitative measure of the non-linearity magnitude in the $\mu(\phi)$ curves. The results show that $\|\mathcal{H}\|$ increases with the applied normal load F_N (rising from 0.005 to 0.017), while $\|\tilde{C}\|$ are close for all normal loads. This indicates an increase of $\|\mathcal{H}\|$ compared to $\|\tilde{C}\|$, indicating that higher loads amplify the non-linearity of the frictional response. In other words, larger values of the tensor $\|\mathcal{H}\|$ were required for the non-linear model to adequately fit the experimental data at higher F_N, thereby minimizing the residuals of the fitted curves. This trend supports a link between the film's non-Coulombic frictional behavior and its anisotropic characteristics, as reflected by the increasingly pronounced deviation of the friction response from the orthogonal axes (0°/180° and 90°/270°).

Furthermore, the 1D mechanical model proposed by Rodrigues et al. [10] does not account for any potential increase in friction coefficients, in relation to $\alpha = 0°$, due to morphological factors. The second identified accommodation mechanism, plastic deformation, only contributes to the reduction of μ. Therefore, the friction behavior and strong anisotropy observed in the film deposited at $\alpha = 40°$ must involve additional mechanisms beyond the porosity and its influence on the deformation modes.

A comparative analysis of the surface morphologies of the films deposited at $\alpha = 30°$, 40°, and 50° reveals that this angular range is critical for Mo films fabricated under the specific GLAD conditions employed in this study. As previously shown in Fig. 2(c) and (e), and Fig. 10, the morphological evolution within the $30° \leq \alpha \leq 50°$ interval is substantial. The structure changes from a dense and compact morphology with a "fish-scale" surface topography at $\alpha = 30°$, to a still dense but randomly oriented and irregularly shaped columnar arrangement at $\alpha = 40°$, and eventually to the emergence of elliptical column tops at $\alpha = 50°$. These observations suggest that the deposition angle range between 35° and 45° may represent a transition zone, where factors other than morphology may play a significant role in determining the frictional behavior.

These observations, combined with the features of its pole figures (Fig. 5), which revealed an inclination of the (110) planes relative to the Mo atom flux, suggest that this film possesses unique characteristics. A more detailed investigation is therefore required to fully understand its behavior.

4. Conclusions

To address whether friction anisotropy is material-dependent for GLAD films, in this study, GLAD molybdenum films were deposited and their frictional behavior was systematically analyzed and compared with that of tungsten (W) films previously studied [10], following an identical methodological approach. Films were deposited at eight different deposition angles ($\alpha = 0°$, 30°, 40°, 50°, 60°, 70°, 80°, and

85°) with thickness of about 500 nm. They were subjected to scratch tests performed in eight directions (defined by the angle ϕ), under four different normal loads (F_N). Based-on the experimental results and the analyses presented above, the main conclusions are summarized as follows:

1. A similar morphological evolution, as the one observed for W films, is observed as the deposition angle (α) increases: The films transition from dense and fibrous structures to columnar morphologies with elliptical-shaped tops aligned along the direction normal to the incoming atom flux, and eventually to "worm-like" columnar structures at the highest α values. This progression is primarily governed by shadowing and fanning effects, which become increasingly dominant at higher deposition angles.
2. As for the W films, Mo films deposited at $\alpha = 0°$, 30°, and $\alpha \geq 50°$ show no significant dependence on the applied normal force during single scratch tests, indicating consistency with Coulomb's law. In contrast, the film deposited at $\alpha = 40°$ deviates from this behavior, exhibiting a clear dependence of the friction coefficient on the applied F_N, thereby indicating non-Coulombic frictional characteristics. This aspect requires an extension of the linear model proposed in [10], adding a non-linear approach, which is proposed in methodology in order to represent a strong non-centrosymmetric anisotropic behavior.
3. Analysis of the polar plots and the anisotropy degree parameter $\overline{\Delta g}$, obtained from the linear model, identifies three distinct categories among the Mo films: (i) Isotropic behavior for $\alpha = 0°$, (ii) slight non-centrosymmetric anisotropy for $\alpha = 30°$, and (iii) orthotropic behavior for $\alpha \geq 50°$. Although some films in the orthotropic group also exhibit non-centrosymmetric results, their dominant anisotropy is characterized by elevated friction coefficients along the $\phi = 90°$ and 270° directions. The highest anisotropy degree ($\overline{\Delta g} = 0.72 \pm 0.06$) was observed for the film deposited at $\alpha = 50°$, followed by a gradual decrease with increasing α, reaching 0.47 ± 0.07 at $\alpha = 85°$. This trend is accompanied by an overall reduction in the friction coefficient at higher deposition angles. Compared with W films [10], the anisotropy degrees of Mo films are considerably higher, as the maximum value reported for W films was 0.35 ± 0. at $\alpha = 70°$. Moreover, although a slight decrease in the overall friction level was observed, it remains negligible compared to that in the present study.
4. As expected based-on the previous studied W films, the frictional behavior of the seven Mo films is strongly correlated with their morphological characteristics. Dense, compact films exhibit isotropic responses. As the morphology moves towards to elongated columns oriented perpendicular to the incident atom flux, column chain structures emerge in these directions. During scratching along $\phi = 90°$ and 270°, the indenter induces rapid contact between adjacent columns, limiting plastic deformation compared to other directions. This reduced deformation corresponds to increased friction coefficients in those directions. Additionally, film morphology governs not only the presence and type of anisotropic frictional behavior, but also its intensity and the overall frictional levels. Increased porosity and the evolution toward "worm-like" column structures minimize column–column interactions and the chain-column effect, thereby contributing to reduced friction coefficients and lower anisotropy degrees ($\overline{\Delta g}$).
5. Film deposited at $\alpha = 40°$ exhibits additional distinct characteristics beyond its deviation from Coulomb's law: A strong non-centrosymmetric friction anisotropy and an atypical morphological structure. The observed anisotropic friction and non-Coulombic behavior appear to be correlated, as the directions showing the greatest deviation from Coulomb's law correspond to those with the highest friction coefficients.

CRediT authorship contribution statement

Guilherme B. Rodrigues: Writing – review & editing, Writing – original draft, Visualization, Software, Methodology, Investigation, Formal analysis, Data curation, Conceptualization. **Pascal Boulet:** Writing – review & editing, Resources, Formal analysis, Data curation. **Nicolas Martin:** Writing – review & editing, Resources, Methodology, Conceptualization. **Fabien Amiot:** Writing – review & editing, Software, Resources, Methodology, Formal analysis, Data curation, Conceptualization. **Guillaume Colas:** Writing – review & editing, Resources, Project administration, Methodology, Funding acquisition, Formal analysis, Data curation, Conceptualization.

Declaration of competing interest

The authors declare that they have no known competing financial interests or personal relationships that could have appeared to influence the work reported in this paper.

Acknowledgments

This work has been achieved in the frame of the EIPHI Graduate school (contract "ANR-17-EURE-0002"). This work is partly supported by the French RENATECH network through its FEMTO-ST technological facilities MIMENTO as well as the FEMTO-ST technological facility AMETISTE.

Appendix A. Supplementary data

Supplementary material related to this article can be found online at https://doi.org/10.1016/j.triboint.2026.111721.

Data availability

Data will be made available on request.

References

[1] Enomoto Y, Tabor D. The frictional anisotropy of diamond. Proc R Soc Lond A 1981;373(1755):405–17. http://dx.doi.org/10.1098/rspa.1981.0001.
[2] Hirano M, Shinjo K, Kaneko R, Murata Y. Anisotropy of frictional forces in muscovite mica. Phys Rev Lett 1991;67(19):2642–6. http://dx.doi.org/10.1103/PhysRevLett.67.2642.
[3] Bohn HF, Federle W. Insect aquaplaning: Nepenthes pitcher plants capture prey with the peristome, a fully wettable water-lubricated anisotropic surface. Proc Natl Acad Sci 2004;101(39):14138–43. http://dx.doi.org/10.1073/pnas.040588510.
[4] Marvi H, Hu DL. Friction enhancement in concertina locomotion of snakes. J R Soc Interface 2012;9(76):3067–80. http://dx.doi.org/10.1098/rsif.2012.0132.
[5] Bauer G, Klein M-C, Gorb SN, Speck T, Voigt D, Gallenmüller F. Always on the bright side: The climbing mechanism of Galium aparine. Proc R Soc Lond B 2011;278(1715):2233–9. http://dx.doi.org/10.1098/rspb.2010.2038.
[6] Zincenko A, Petrovskii S, Volpert V, Banerjee M. Turing instability in an economic–demographic dynamical system may lead to pattern formation on a geographical scale. J R Soc Interface 2021;18(177):1–16. http://dx.doi.org/10.1098/rsif.2021.0034.
[7] Chen G, Zhang Z, Wu J, Zhang B, Chu Z, Cui J. A novel methodology for intrinsic adhesion state sensing in gecko-inspired directional dry adhesives. Sensors Actuators A 2024;374(115492):1–10. http://dx.doi.org/10.1016/j.sna.2023.115492.
[8] Robbie K, Friedrich L, Dew S, Smy T, Brett M. Fabrication of thin films with highly porous microstructures. J Vac Sci Technol A 1995;13(3):1032–5. http://dx.doi.org/10.1116/1.579579.
[9] Hawkeye MM, Taschuk MT, Brett MJ. Glancing angle deposition of thin films: Engineering the nanoscale. 1st ed.. John Wiley & Sons; 2014.
[10] Rodrigues GB, Martin N, Amiot F, Colas G. Friction anisotropy dependence on morphology of GLAD W films. Tribol Int 2025;206:110556. http://dx.doi.org/10.1016/j.triboint.2025.110556.
[11] Mohanty B, Morton BD, Alagoz AS, Karabacak T, Zou M. Frictional anisotropy of tilted molybdenum nanorods fabricated by glancing angle deposition. Tribol Int 2014;80:216–21. http://dx.doi.org/10.1016/j.triboint.2014.07.010.

[12] Krishnan R, Riley M, Lee S, Lu T-M. Vertically aligned biaxially textured molybdenum thin films. J Appl Phys 2011;110(6). http://dx.doi.org/10.1063/1.3638452.
[13] Chen L, Lu T-M, Wang G-C. Incident flux angle induced crystal texture transformation in nanostructured molybdenum films. J Appl Phys 2012;112(2):024303. http://dx.doi.org/10.1063/1.4737877.
[14] Li Z-H, Cho E-S, Kwon SJ. Molybdenum thin film deposited by in-line DC magnetron sputtering as a back contact for Cu (In, Ga) Se2 solar cells. Appl Surf Sci 2011;257(22):pp. 9682–9688. http://dx.doi.org/10.1016/j.apsusc.2011.06.101.
[15] Braun S, Mai H, Moss M, Scholz R, Leson A. Mo/Si multilayers with different barrier layers for applications as extreme ultraviolet mirrors. Japan J Appl Phys 2002;41(6S):4074. http://dx.doi.org/10.1143/JJAP.41.4074.
[16] Mostako A, Khare A. Molybdenum thin films via pulsed laser deposition technique for first mirror application. Laser Part Beams 2012;30(4):559–67. http://dx.doi.org/10.1017/S0263034612000560.
[17] Aqil MM, Azam MA, Aziz MF, Latif R. Deposition and characterization of molybdenum thin film using direct current magnetron and atomic force microscopy. J Nanotechnol 2017;2017:4862087. http://dx.doi.org/10.1155/2017/4862087.
[18] Liu S, Peyronnel A, Wang Q, Keer L. An extension of the Hertz theory for three-dimensional coated bodies. Tribol Lett 2005;18:303–14. http://dx.doi.org/10.1007/s11249-005-9002-8.
[19] Coulomb CA. Théorie des machines simples: en ayant égard au frottement de leurs parties, et à la roideur de cordages, vol. 10, 1785, p. 161–331.
[20] Zmitrowicz A. A theoretical model of anisotropic dry friction. Wear 1981;73(1):9–39. http://dx.doi.org/10.1016/0043-1648(81)90207-6.
[21] Zmitrowicz A. Illustrative examples of centrosymmetric and non-centrosymmetric anisotropic friction. Int J Solids Struct 1992;29(23):3045–59. http://dx.doi.org/10.1016/0020-7683(92)90157-O.
[22] Zmitrowicz A. Mathematical descriptions of anisotropic friction. Int J Solids Struct 1989;25(8):837–62. http://dx.doi.org/10.1016/0020-7683(89)90034-6.
[23] Nieuwenhuizen J, Haanstra H. Microfractography of thin films. Philips Tech Rev 1966;27(3):87–91.
[24] Tait R, Smy T, Brett M. Modelling and characterization of columnar growth in evaporated films. Thin Solid Films 1993;226(2):196–201. http://dx.doi.org/10.1016/0040-6090(93)90457-N.
[25] Zhao Y, He Y, Brown C. Composition dependent nanocolumn tilting angle during the oblique angle co-deposition. Appl Phys Lett 2012;100(3):033106. http://dx.doi.org/10.1063/1.3675894.
[26] El Beainou R, Cote J-M, Tissot V, Potin V, Martin N. Resistivity anisotropy of tilted columnar W and WCu thin films. Surf Coat Technol 2021;421:127412. http://dx.doi.org/10.1016/j.surfcoat.2021.127412.
[27] Pedrosa P, Ferreira A, Cote J-M, Martin N, Yazdi MAP, Billard A, Lanceros-Mendez S, Vaz F. Influence of the sputtering pressure on the morphological features and electrical resistivity anisotropy of nanostructured titanium films. Appl Surf Sci 2017;420:681–90. http://dx.doi.org/10.1016/j.apsusc.2017.05.215.
[28] Boukhalfa H, Potin V, Martin N. Microstructural analysis and electrical behaviours of co-sputtered W–Ag thin films with a tilted columnar architecture. J Phys D: Appl Phys 2021;54(25):255304. http://dx.doi.org/10.1088/1361-6463/ac06de.
[29] Chargui A, El Beainou R, Mosset A, Euphrasie S, Potin V, Vairac P, Martin N. Influence of thickness and sputtering pressure on electrical resistivity and elastic wave propagation in oriented columnar tungsten thin films. Nanomaterials 2020;10(1):81. http://dx.doi.org/10.3390/nano10010081.
[30] Chargui A, El Beainou R, Mosset A, Gavoille J, Vairac P, Euphrasie S, Martin N. Anisotropic thermal conductivity of nanocolumnar W thin films. Phys Lett A 2022;426:127878. http://dx.doi.org/10.1016/j.physleta.2021.127878.
[31] El Beainou R, Salut R, Robert L, Cote J-M, Potin V, Martin N. Anisotropic conductivity enhancement in inclined W-Cu columnar films. Mater Lett 2018;232:126–9. http://dx.doi.org/10.1016/j.matlet.2018.08.120.
[32] Potin V, Boukhalfa H, Martin N. Oblique angle co-deposition of nanocolumnar tungsten thin films with two W sources: Effect of pressure and target current. Mater Chem Phys 2022;281:125864. http://dx.doi.org/10.1016/j.matchemphys.2022.125864.
[33] Siad A, Besnard A, Nouveau C, Jacquet P. Critical angles in DC magnetron glad thin films. Vacuum 2016;131:p305–311. http://dx.doi.org/10.1016/j.vacuum.2016.07.012.
[34] Krishnan R, Riley M, Lee S, Lu T-M. Formation of biaxially textured molybdenum thin films under the influence of recrystallization conditions. Thin Solid Films 2011;519(16):5429–32. http://dx.doi.org/10.1016/j.tsf.2011.02.048.
[35] Gordillo G, Grizález M, Hernandez L. Structural and electrical properties of DC sputtered molybdenum films. Sol Energy Mater Sol Cells 1998;51(3–4):327–37. http://dx.doi.org/10.1016/S0927-0248(97)00236-5.
[36] Liedtke-Grüner S, Grüner C, Lotnyk A, Gerlach JW, Mensing M, Schumacher P, Rauschenbach B. Crystallinity and texture of molybdenum thin films obliquely deposited at room temperature. Thin Solid Films 2019;685:8–16. http://dx.doi.org/10.1016/j.tsf.2019.06.041.
[37] Shen Y. Effect of deposition conditions on mechanical stresses and microstructure of sputter-deposited molybdenum and reactively sputter-deposited molybdenum nitride films. Mater Sci Eng A 2003;359(1–2):158–67. http://dx.doi.org/10.1016/S0921-5093(03)00336-8.
[38] Chelvanathan P, Shahahmadi S, Arith F, Sobayel K, Aktharuzzaman M, Sopian K, Alharbi F, Tabet N, Amin N. Effects of RF magnetron sputtering deposition process parameters on the properties of molybdenum thin films. Thin Solid Films 2017;638:213–9. http://dx.doi.org/10.1016/j.tsf.2017.07.057.
[39] Minkin A, Kozlov V. Preferred growth of molybdenum thin films during magnetron sputtering. J Solid State Chem 2021;304:122543. http://dx.doi.org/10.1016/j.jssc.2021.122543.
[40] So E, Demirel MC, Wahl KJ. Mechanical anisotropy of nanostructured parylene films during sliding contact. J Phys D Appl Phys 2010;43(4):045403. http://dx.doi.org/10.1088/0022-3727/43/4/045403.
[41] Hirakata H, Nishihira T, Yonezu A, Minoshima K. Frictional anisotropy of oblique nanocolumn arrays grown by glancing angle deposition. Tribol Lett 2011;44:259–68. http://dx.doi.org/10.1007/s11249-011-9764-0.
[42] Mohanty B, Ivanoff TA, Alagoz AS, Karabacak T, Zou M. Study of the anisotropic frictional and deformation behavior of surfaces textured with silver nanorods. Tribol Int 2015;92:439–45. http://dx.doi.org/10.1016/j.triboint.2015.06.007.
[43] Pandey M, Verma D, Balakrishnan V, Gosvami NN, Singh J. Frictional anisotropy of Ag nanocolumnar surfaces. Tribol Int 2021;153:106674. http://dx.doi.org/10.1016/j.triboint.2020.106674.
[44] Yang W, Sherman VR, Gludovatz B, Mackey M, Zimmermann EA, Chang EH, Schaible E, Qin Z, Buehler MJ, Ritchie RO. Protective role of Arapaima gigas fish scales: Structure and mechanical behavior. Acta Biomater 2014;10(8):3599–614. http://dx.doi.org/10.1016/j.actbio.2014.04.009.
[45] Ali H, Ebrahimi H, Ghosh R. Frictional damping from biomimetic scales. Sci Rep 2019;9(1):14628. http://dx.doi.org/10.1038/s41598-019-50944-0.
[46] Rong W, Zhang H, Zhang T, Mao Z, Liu X, Song K. Drag reduction using lubricant-impregnated anisotropic slippery surfaces inspired by bionic fish scale surfaces containing micro-/nanostructured arrays. Adv Eng Mater 2021;23(1):2000821. http://dx.doi.org/10.1002/adem.202000821.
[47] Ji Z, Yan C, Ma S, Gorb S, Jia X, Yu B, Wang X, Zhou F. 3D printing of bioinspired topographically oriented surfaces with frictional anisotropy for directional driving. Tribol Int 2019;132:99–107. http://dx.doi.org/10.1016/j.triboint.2018.12.010.
[48] Vick D, Smy T, Brett M. Growth behavior of evaporated porous thin films. J Mater Res 2002;17(11):2904–11. http://dx.doi.org/10.1557/JMR.2002.0391.
[49] El Beainou R, Chargui A, Pedrosa P, Mosset A, Euphrasie S, Vairac P, Martin N. Electrical resistivity and elastic wave propagation anisotropy in glancing angle deposited tungsten and gold thin films. Appl Surf Sci 2019;475:606–14. http://dx.doi.org/10.1016/j.apsusc.2019.01.166.
[50] Martin N, Sauget J, Nyberg T. Anisotropic electrical resistivity during annealing of oriented columnar titanium films. Mater Lett 2013;105:20–3. http://dx.doi.org/10.1016/j.matlet.2013.03.049.